

Double-waveguide quantum cascade laser

Romain Blanchard, Cécile Grezes, Stefan Menzel, Christian Pflügl, Laurent Diehl et al.

Citation: *Appl. Phys. Lett.* **100**, 033502 (2012); doi: 10.1063/1.3678033

View online: <http://dx.doi.org/10.1063/1.3678033>

View Table of Contents: <http://apl.aip.org/resource/1/APPLAB/v100/i3>

Published by the [American Institute of Physics](#).

Related Articles

Improvement of hole injection and electron overflow by a tapered AlGaIn electron blocking layer in InGaIn-based blue laser diodes

Appl. Phys. Lett. **100**, 031105 (2012)

Improvement of temperature-stability in a quantum well laser with asymmetric barrier layers

Appl. Phys. Lett. **100**, 021107 (2012)

444.9nm semipolar (112) laser diode grown on an intentionally stress relaxed InGaIn waveguiding layer

Appl. Phys. Lett. **100**, 021104 (2012)

Effects of stimulated emission on transport in terahertz quantum cascade lasers based on diagonal designs

Appl. Phys. Lett. **100**, 011108 (2012)

Single lateral mode mid-infrared laser diode using wavelength-scale modulation of the facet reflectivity

Appl. Phys. Lett. **100**, 011103 (2012)

Additional information on *Appl. Phys. Lett.*

Journal Homepage: <http://apl.aip.org/>

Journal Information: http://apl.aip.org/about/about_the_journal

Top downloads: http://apl.aip.org/features/most_downloaded

Information for Authors: <http://apl.aip.org/authors>

ADVERTISEMENT

**AIP**Advances

Submit Now

**Explore AIP's new
open-access journal**

- **Article-level metrics
now available**
- **Join the conversation!
Rate & comment on articles**

Double-waveguide quantum cascade laser

Romain Blanchard,¹ Cécile Grezes,¹ Stefan Menzel,¹ Christian Pflügl,^{1,2} Laurent Diehl,^{1,2} Yong Huang,³ Jae-Hyun Ryou,³ Russell D. Dupuis,³ and Federico Capasso^{1,a)}

¹*School of Engineering and Applied Sciences, Harvard University, 29 Oxford St., Cambridge, Massachusetts 02138, USA*

²*Eos Photonics Inc., 30 Spinelli Place, Cambridge, Massachusetts 02138, USA*

³*Center for Compound Semiconductors and School of Electrical and Computer Engineering, Georgia Institute of Technology, 777 Atlantic Dr. NW, Atlanta, Georgia 30332, USA*

(Received 5 November 2011; accepted 21 December 2011; published online 18 January 2012)

We demonstrate 1.1 W peak power at room-temperature from a double-waveguide quantum cascade laser (QCL) grown by metal-organic chemical vapor deposition. Two full broadband QCL active regions were grown on top of each other separated by thick cladding layers to reduce gain competition. Simultaneous lasing on Fabry-Perot modes separated by as much as 360 cm^{-1} is obtained. This design paves the way for high-brightness broadband mid-infrared sources, as well as more complex three-terminal devices. © 2012 American Institute of Physics.

[doi:10.1063/1.3678033]

Quantum cascade lasers (QCLs) are near-ideal mid-infrared semiconductor light sources, combining wavelength agility¹ and operation at room temperature with continuous-wave watt-level output power.² They enable the coverage of the mid-infrared region of the electromagnetic spectrum which is of great importance for many applications, from free space communication to chemical sensing.³ In an effort to obtain a broad spectral coverage, tunable broadband QCLs have been developed, with a single lasing frequency scanned over the gain spectrum.^{4–6} However, some applications would require *simultaneous* broadband lasing. In particular, Fourier-transform infrared (FTIR) spectrometers, which are widely used chemical analysis tools, still rely on thermal radiation sources. The low infrared power from these sources restricts the use of FTIR spectrometers to low-absorptivity samples. Developing broadband QCLs as sources for FTIR spectrometers would enable new applications, such as solvent-based process monitoring.⁷

The basic strategy to obtain broadband lasing in QCLs consists of stacking in series active regions operating at different wavelengths, in order to form a heterocascade⁸ with a wide composite gain spectrum. Ultra-broad gain from a single active region was also recently achieved.^{9,10} Lasing mode proliferation across the gain spectrum¹¹ is then enabled by a low threshold for the spatial hole burning instability in QCLs.¹² Simultaneous lasing over a range as wide as 360 cm^{-1} with a small gap of 36 cm^{-1} has been reported.⁴ However, broadband simultaneous lasing remains very challenging because of the need to achieve a flat net gain spectrum in order to ensure that all lasing wavelengths have the same threshold.

We present here a waveguide structure designed to obtain broad and bright emission from a single monolithic device by growing two full QCLs, each with its own optical waveguide, on top of each other. Contrary to previous works using indium phosphide (InP) inter-stacks in a QCL struc-

ture,^{13,14} the thick InP spacer used in this work to separate the active regions of the two QCLs is intended to create two uncoupled optical waveguides. We demonstrate excellent room temperature performance from this device grown by metal-organic chemical vapor deposition¹⁵ (MOCVD). The ability to grow thick QCL structures by MOCVD is particularly interesting for industrial production prospects since the growth of such complex structures in a single growth run can significantly reduce manufacturing costs. The device demonstrated here offers the advantages of a small footprint in addition to a small and reliable spacing between active regions, enabling to obtain good beam quality, for example, using a microlens array.

In order to maximize the spectral coverage of the device, we distribute four different cascade designs over the two gain media (see Fig. 1). All cascades are based on a bound-to-continuum design,¹⁶ characterized by an inherently broad gain spectrum, centered respectively at 135, 145, 165, and 175 meV, (in wavenumbers: 1089, 1170, 1331, and 1411 cm^{-1}). In order to reduce gain competition,¹⁷ which increases with increasing overlap of the gain curves, spectrally adjacent active regions were separated from each other.

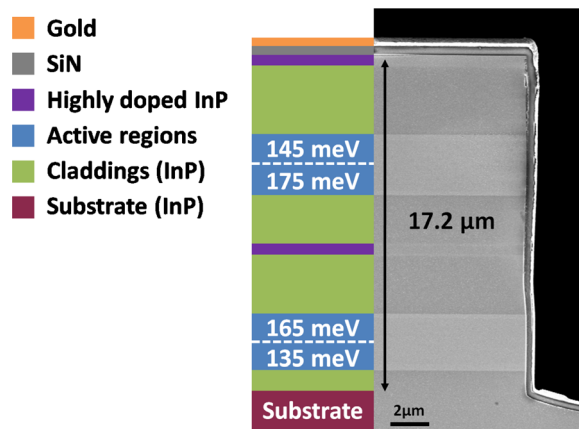


FIG. 1. (Color online) Schematic of the waveguide structure and scanning electron microscope (SEM) image.

^{a)}Author to whom correspondence should be addressed. Electronic mail: capasso@seas.harvard.edu.

The number of stages for each wavelength was adjusted in an attempt to obtain a flat net gain spectrum. The layer sequence of the structure is described in note, Ref. 18. A low doping is used for the layers next to the gain media, in order to reduce free-carrier absorption. We reduce the coupling between the two waveguides, first by having a thick cladding between them and second by inserting a highly doped plasmon layer to attenuate the far-reaching evanescent tails.

Round mesas with a $200\ \mu\text{m}$ diameter were processed for the measurement of the electro-luminescence (EL) spectra. A broad EL spectrum spanning $1025\text{--}1475\ \text{cm}^{-1}$ is obtained for the full double-waveguide structure, as shown in Fig. 2(a). We etched away the upper waveguide, down to the middle of the spacer separating the two waveguides, and reprocessed some mesas in order to measure the EL from the lower waveguide only. From the difference between the spectrum measured for the full structure and the lower waveguide only, we deduced the spectrum for the EL of the upper waveguide only. We observe two EL peaks for each waveguide, at $1070\ \text{cm}^{-1}$ and $1310\ \text{cm}^{-1}$ for the lower one (measured) and at $1170\ \text{cm}^{-1}$ and $1390\ \text{cm}^{-1}$ for the upper one (calculated). For both waveguides, the long-wavelength peak

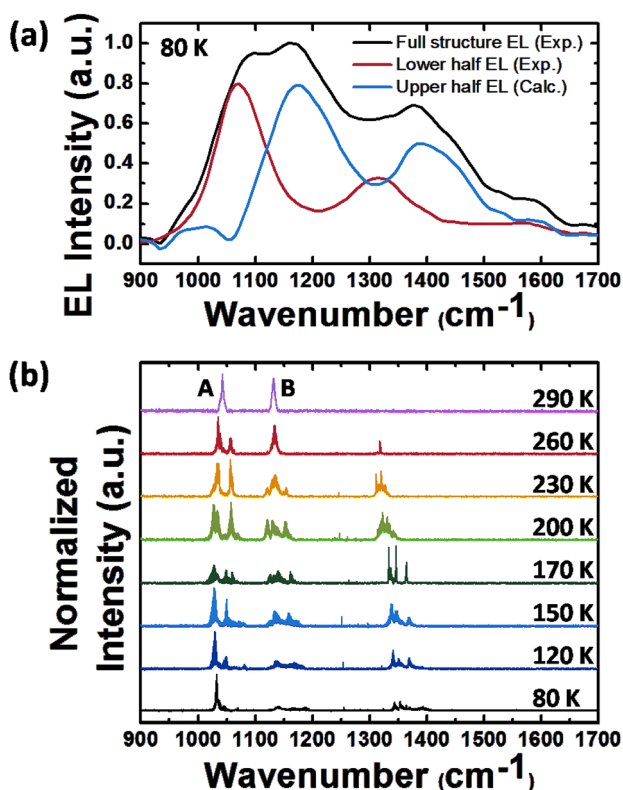


FIG. 2. (Color online) (a) Measured EL spectra at 80 K from the full double-waveguide structure (black curve) and from the lower waveguide only (red curve), with upper waveguide etched away. Calculated difference of the two spectra as an approximation of the EL from the upper waveguide only (blue curve). The measured spectra are taken for two cleaved mesas of similar sizes with similar current ($\approx 1.4\ \text{A}$) flowing through them. The corresponding bias for the full structure is $\approx 20\ \text{V}$, comparable to the 19 V bias used for the lasing spectra in (b). EL is shown at 80 K for direct comparison with the lasing spectrum at 80 K. (b) Lasing spectra at different temperatures for a $23\ \mu\text{m}$ wide and 3 mm long laser, operated in pulsed mode (100 ns, 20 kHz). The laser is driven at a constant bias of 19 V (current $\approx 2\ \text{A}$). A high-reflectivity coating was deposited on the back facet of the laser. The letters A and B allow identification of the two groups of modes.

is about twice as strong as the short-wavelength peak. We believe that this can be explained by resonant cross-absorption of the short wavelengths in the long-wavelength stages, resulting in a significantly lower net gain at short wavelengths. We identified two transitions that can lead to a strong absorption of the short wavelength. One is from the upper lasing state to a high energy level in the active region quantum wells, close to the continuum. The second is from the lower laser state to the level above the upper laser state. While gathering spectrally adjacent stages in the same waveguide could reduce cross-absorption, it would increase gain competition. For this reason, cross-absorption would be better addressed with a careful design of the stages. In future work, we will focus on improving the designs of the individual active regions, in particular by implementing innovative solutions for broadband lasing.⁴ The combination of these proven broadband designs^{4,9,10} with our double-waveguide QCL approach is a straightforward path towards monolithic QCL sources with unprecedented lasing bandwidth.

Fabrication of the lasers started with the etching of $17\ \mu\text{m}$ -deep trenches by reactive ion etching (RIE) using a photolithography-defined SU8 mask. The side-walls remain straight and smooth over the whole depth, as seen in Fig. 1. The trenches defined waveguides 20, 23, and $26\ \mu\text{m}$ -wide. A 300 nm-thick SiN insulation layer was then deposited by plasma-enhanced chemical vapor deposition and opened by RIE on top of the laser ridges. Top and bottom metallization consisted of Ti(15 nm) and Au(450 nm) layers. The fabricated devices were cleaved to 3 mm length, high-reflection coated ($\text{Al}_2\text{O}_3/\text{Au}$) on the back facet and indium mounted epi-side up on copper heat sinks. The devices were characterized in pulsed operation with 100 ns pulse width and 20 kHz repetition rate.

Fig. 2(b) shows lasing spectra obtained at different operating temperatures. Up to 260 K, a temperature that can be reached with thermoelectric coolers, we can distinguish three main islands of Fabry-Perot modes, with lasing modes separated by up to $360\ \text{cm}^{-1}$. For temperatures above 260 K, only the two long-wavelength islands survive. They are positioned where maximum luminescence is observed (see Fig. 2(a)). We note that for lasers processed from a piece of wafer containing only the lower active region, only the group of modes A is lasing. Together with the luminescence data, this indicates that the group of modes B is lasing mainly in the upper waveguide where it experiences the most gain, whereas the group of modes A is lasing mainly in the lower waveguide.

The light-current-voltage characteristics shown in Fig. 3(a) demonstrate good lasing performance from both gain media, at room temperature and in pulsed operation (100 ns/20 kHz). Using a short-pass filter at $9.3\ \mu\text{m}$ (between the group of modes A and B), we observed that the threshold is the same for both groups of modes and that the power is approximately equally divided between them. This indicates that both waveguides have comparable optical losses. Remarkably, the good performance of the device, in particular of the group of modes B for which gain is provided by the last stages grown, indicates that high quality growth can be sustained for such thick structure and that our waveguide design maintains low optical losses.

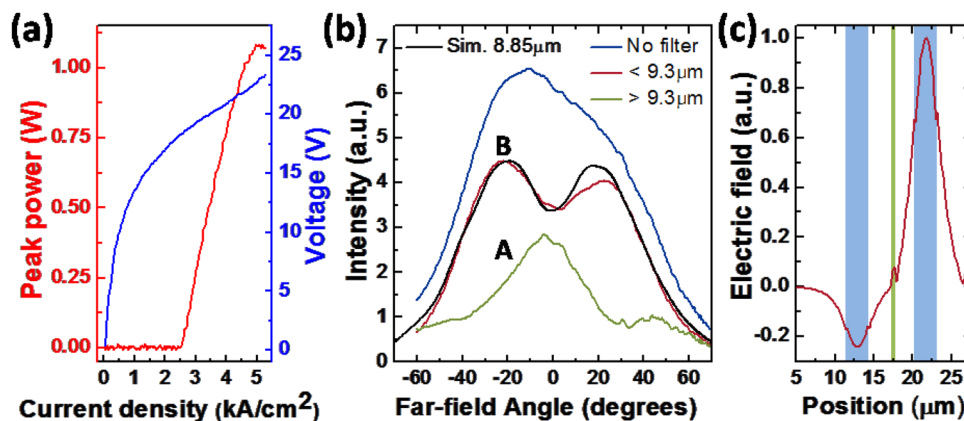


FIG. 3. (Color online) (a) Light intensity (peak power) (red) and voltage (blue) versus current density for a representative device (with high-reflectivity coating) operated in pulsed mode (100 ns, 20 kHz) at room temperature. (b) Far-field of the representative device of Fig. 2(b), operated in the same conditions. In blue, without filter; in red, with a short-pass filter at $9.3\ \mu\text{m}$. In green, the calculated difference of the two previous curves (blue minus red), illustrating the far-field of modes A. In black, simulated far-field of the linear combination of the two lowest-order orthogonal TM waveguide modes fitting best to the experimental data. The simulations are done at the central wavelength of the group of modes B ($8.85\ \mu\text{m}$). The far-fields are measured by scanning a mercury-cadmium-telluride detector located 10 cm away from the laser, along a direction perpendicular to the growth planes. (c) Instantaneous electric field (at a time maximizing field amplitude) across the structure, along the direction perpendicular to the layer planes. The two active regions are in light blue, the central plasmon layer in green and the top gold contact in yellow.

To investigate optical coupling between the two waveguides, we measured the far-field of a representative laser operated at room-temperature. Fig. 3(b) shows line-scans along the direction perpendicular to the layer planes. We observe that the emission of the group of modes B features two peaks separated by a shallow dip. Using finite-difference simulations (Lumerical FDTD), we solved for the two lowest-order orthogonal TM modes supported by the double-waveguide structure. We then computed the far-fields (obtained by near-field to far-field transformations) of linear combinations of these two modes in order to identify the superposition corresponding best to the experimental far-field. The best fit is shown in black in Fig. 3(b), and the corresponding mode profile is shown in Fig. 3(c). The intensity is mostly confined to the upper waveguide, with only about 6% of the power in the lower waveguide. The two lobes of the electric field in the two waveguides are π -shifted one with respect to the other. Lasing on such mode is favoured as it corresponds to a minimum of field at the center of the spacer region where we introduced a highly doped lossy layer. A thicker highly-doped layer with a larger doping level between the two active regions could easily reduce the coupling between the two waveguides. In contrast, the far-field calculated for the group of modes A indicates that light is emitted mainly from one waveguide, the lower waveguide in our case.

In summary, we have presented a double-waveguide QCL design. This small-footprint design provides flexibility to distribute multiple QCL stages over two weakly coupled optical waveguides, in order to obtain broadband emission while dealing with common issues of heterocascade QCLs, such as cross-absorption and gain competition. We demonstrated that good room temperature performance is preserved with this very thick device grown by MOCVD. Full decoupling of the waveguides was not achieved at all wavelengths, but this can easily be accomplished by increasing the thickness and/or doping of the cladding layers. Furthermore, intentional coupling of the two waveguides can be explored to obtain beam-steering of the laser emission. Our design

also opens the route to more complex three-terminal devices by using the highly doped plasmon layer separating the two waveguides as a third contact.

We acknowledge support from DTRA (Grant No. HDTRA1-10-1-0031-DOD) and partial financial support from Hamamatsu Photonics KK. This work was performed in part at the Center for Nanoscale Systems (CNS) at Harvard University, a member of NNIN, which is supported by the NSF. R.D. would like to thank the support of the Steve W. Chaddick Endowed Chair of Opto-Electronics at Georgia Tech. We thank M. A. Kats and P. Genevet for helpful discussions.

¹F. Capasso, C. Gmachl, R. Paiella, A. Tredicucci, A. L. Hutchinson, D. L. Sivco, J. N. Baillargeon, A. Y. Cho, and H. C. Liu, *IEEE J. Sel. Top. Quantum Electron.* **6**, 931 (2000).

²A. Lyakh, R. Maulini, A. Tsekoun, R. Go, S. Von der Porten, C. Pflügl, L. Diehl, F. Capasso, and K. N. Patel, *Proc. Natl. Acad. Sci. U.S.A.* **107**, 18799 (2010).

³R. F. Curl, F. Capasso, C. Gmachl, A. A. Kosterev, B. McManus, R. Lewicki, M. Pusharsky, G. Wysocki, and F. K. Tittel, *Chem. Phys. Lett.* **487**, 1 (2010).

⁴A. Hugi, R. Terazzi, Y. Bonetti, A. Wittmann, M. Fischer, M. Beck, J. Faist, and E. Gini, *Appl. Phys. Lett.* **95**, 061103 (2009).

⁵B. G. Lee, M. A. Belkin, C. Pflügl, L. Diehl, H. Zhang, R. Audet, J. MacArthur, D. Bour, S. Corzine, G. Hoffer *et al.*, *IEEE J. Quantum Electron.* **45**, 554 (2009).

⁶E. Mujagic, C. Schwarzer, Y. Yao, J. Chen, C. Gmachl, and G. Strasser, *Appl. Phys. Lett.* **98**, 141101 (2011).

⁷L. Diehl, C. Pflügl, M. Witinski, P. Wang, T. Tague, and F. Capasso, in *CLEO: Applications* (Optical Society of America, 2010), paper JThB1.

⁸C. Gmachl, D. L. Sivco, J. N. Baillargeon, A. L. Hutchinson, F. Capasso, and A. Y. Cho, *Appl. Phys. Lett.* **79**, 572 (2001).

⁹K. Fujita, T. Edamura, S. Furuta, and M. Yamanishi, *Appl. Phys. Lett.* **96**, 241107 (2010).

¹⁰Y. Yao, X. Wang, J.-Y. Fan, and C. Gmachl, *Appl. Phys. Lett.* **97**, 081115 (2010).

¹¹C. Gmachl, D. L. Sivco, R. Colombelli, F. Capasso, and A. Y. Cho, *Nature* **415**, 883 (2002).

¹²A. Gordon, C. Y. Wang, L. Diehl, F. X. Kartner, A. Belyanin, D. Bour, S. Corzine, G. Hoffer, H. C. Liu, H. Schneider *et al.*, *Phys. Rev. A* **77**, 53804 (2008).

¹³A. Bismuto, T. Gresch, A. Bächle, and J. Faist, *Appl. Phys. Lett.* **93**, 231104 (2008).

- ¹⁴J. Liu, F. Liu, L. Li, L. Wang, and Z. Wang, *Semicond. Sci. Technol.* **24**, 075023 (2009).
- ¹⁵Y. Huang, J.-H. Ryou, R. D. Dupuis, C. Pflügl, F. Capasso, K. Sun, A. M. Fischer, and F. A. Ponce, *J. Cryst. Growth* **316**, 75 (2010).
- ¹⁶J. Faist, M. Beck, T. Aellen, and E. Gini, *Appl. Phys. Lett.* **78**, 147 (2001).
- ¹⁷M. Geiser, C. Pflügl, A. Belyanin, Q. J. Wang, N. Yu, T. Edamura, M. Yamashita, H. Kan, M. Fischer, A. Wittmann *et al.*, *Opt. Express* **18**, 9900 (2010).
- ¹⁸Layer sequence: InP (1.5 μm , $5.10^{16} \text{ cm}^{-3}$)/InGaAs (300 nm, $n_1 = 3.10^{16} \text{ cm}^{-3}$)/first active region (22 cascades at $\lambda = 9.12 \mu\text{m}$ and 15 cascades at $\lambda = 7.05 \mu\text{m}$)/InGaAs (300 nm, n_1)/InP (3 μm , $3.10^{16} \text{ cm}^{-3}$)/InP (500 nm, $1.10^{19} \text{ cm}^{-3}$)/InP (2.5 μm , $3.10^{16} \text{ cm}^{-3}$)/InGaAs (200 nm, n_1)/second active region (20 cascades at $\lambda = 6.33 \mu\text{m}$ and 19 cascades at $\lambda = 7.95 \mu\text{m}$)/InGaAs (300 nm, n_1)/InP (1.5 μm , $5.10^{16} \text{ cm}^{-3}$)/InP (2 μm , $1.10^{17} \text{ cm}^{-3}$)/InP (500 nm, $1.10^{19} \text{ cm}^{-3}$)/InGaAs (20 nm, $1.10^{19} \text{ cm}^{-3}$).